Amelogenin Affects Brushite Crystal Morphology and Promotes Its Phase Transformation to Monetite

Dongni Ren[a], Qichao Ruan[a], Jinhui Tao[b], Jonathan Lo[c], Steven Nutt[c], and Janet Moradian-Oldak[a]*

[a] Center for Craniofacial Molecular Biology, Herman Ostrow School of Dentistry, University of Southern California, Los Angeles, California 90033,United States
[b] Physical Sciences Division, Pacific Northwest National Laboratory, Richland, Washington 99352, United States
[c] Mork Family Department of Chemical Engineering and Materials Science, University of Southern California, Los Angeles, California 90089, United States

* E-mail: joldak@usc.edu. Tel: 323-442-1759. Fax: 323-442-2981

Abstract:

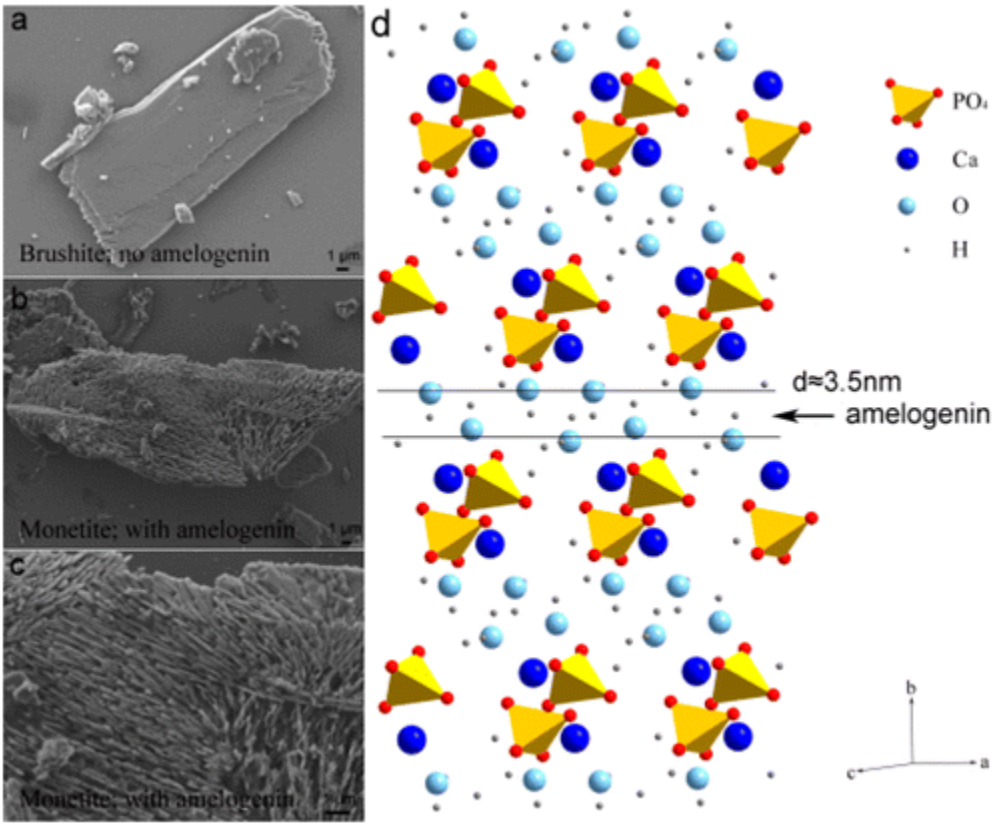

Amelogenin protein is involved in organized apatite crystallization during enamel formation. Brushite ($CaHPO_4 \cdot 2H_2O$), one of the precursors of hydroxyapatite mineralization *in*

Ren, Dongni; Ruan, Qichao; Tao, Jinhui; Lo, Jonathan; Nutt, Steven; Moradian-Oldak, Janet, **"Amelogenin affects brushite crystal morphology and promotes its phase transformation to monetite"** Crystal Growth & Design Aug 16 [9] 4981-90 (2016) DOI: **10.1021/acs.cgd.6b00569**

vitro, has been used for fabrication of biomaterials for hard tissue repair. In order to explore its potential application in biomimetic material synthesis, we studied the influence of the enamel protein amelogenin on brushite morphology and phase transformation to monetite. Our results show that amelogenin can adsorb onto the surface of brushite, leading to the formation of layered morphology on the (010) face. Amelogenin promoted the phase transformation of brushite into monetite ($CaHPO_4$) in the dry state, presumably by interacting with crystalline water layers in brushite unit cells. Changes to the crystal morphology mediated by amelogenin continued even after the phase transformation from brushite to monetite, leading to the formation of organized platelets with an interlocked structure. This effect of amelogenin on brushite morphology and the phase transformation to monetite could provide a new approach to developing biomimetic materials.

1. INTRODUCTION

Enamel is the outermost layer of the mammalian tooth and is considered to be one of the hardest calcium phosphate-containing bioceramics.(1) This calcified tissue is comprised of more than 85 v/v % (or 98 wt %) hydroxyapatite (HA) crystals and, being closely connected to the underlying dentin, shows exceptional biological and mechanical properties.(2, 3) The high wear- and fracture-resistance of enamel is associated with the highly ordered structure of enamel prisms (rods) and the interwoven arrangement of HA that produces interprismatic enamel.(4-6) The formation of the basic building blocks of enamel, long and thin HA crystals, is mediated by the components of the extracellular matrix secreted by the ameloblast cells.(7) Among the matrix proteins, amelogenin is the most prevalent and is essential for normal enamel formation.(8, 9) It is well accepted that amelogenin plays critical roles in regulating enamel crystal morphology and

organization through its specific interaction with forming enamel crystals. In order to get better insight into the function of amelogenin in mediating mineral formation in enamel, investigators have used in vitro models to study interactions between amelogenin and calcium phosphate crystals, including hydroxyapatite and octacalcium phosphate.(10-12) In contrast, there has been little study of how amelogenin may mediate brushite (dicalcium phosphate dehydrate, DCPD, $CaHPO_4 \cdot 2H_2O$) or monetite (dicalcium phosphate anhydrate, $CaHPO_4$) crystal growth.

Brushite and monetite are metastable phases of calcium orthophosphate. Brushite crystals consist of parallel Ca-PO_4 chains that are held together by lattice water molecules via hydrogen bonds.(13) The loss of crystal water results in the transformation from brushite into anhydrous monetite. The complete dehydration of brushite usually requires heating at a relatively high temperature, over 200 °C.(14) Owing to their thermodynamic metastability under physiological conditions,(15-17) both brushite and monetite have been considered suitable for developing calcium phosphate biomaterials.(18-20) Several studies on the application of brushite for fabricating cements for bone and tooth repair have been reported. Kumar et al. used single brushite crystals as seeds for the growth of hydroxyapatite layers as implant materials.(21) Biemond et al. reported that a biomimetic brushite coating on an implant enhanced bone ingrowth significantly.(22) There have been several reports on biomimetic approaches for bone tissue engineering using monetite together with hydroxyapatite. Hsu et al. reported the growth of monetite crystals with diverse morphologies on top of hydroxyapatite under hydrothermal conditions.(23) Using a liquid crystal matrix and the concept of a mineral bridge, He et al. successfully synthesized monetite with superstructures similar to the mineral bridge in natural biominerals.(24) While biomaterials with potential application in hard tissue repair have been

developed, in most of these reports extreme conditions far from those of physiological environments were used, including high temperatures (above 200 °C) and/or extreme pH values.

Brushite and monetite are effective starting materials in the preparation of various nanostructured hydroxyapatite crystals.(25, 26) For example, nanoneedles, fibers, and sheets of hydroxyapatite have been prepared by the hydrolysis of monetite in alkali solutions by varying the pH and ion concentrations. Using a single monetite crystal as a template, enamel-like hydroxyapatite was obtained in an alkaline aqueous solution with the assistance of microwave irradiation(27) or mediation by organic molecules.(28) Recently, we have successfully synthesized a layered monetite–chitosan composite that can further transform into a hydroxyapatite composite with a multilevel ordered structure.(29) These studies demonstrated that the structural control of brushite and monetite precursors by organic molecules is important in the construction of multilevel hierarchical hydroxyapatite.

In the present work, considering the role of the amelogenin protein in controlling in vitro calcium phosphate crystal formation and its potential application in biomaterial synthesis, we studied the effect of amelogenin on brushite crystal morphology and the subsequent phase transformation to monetite. We demonstrated that in a dry state, at mild temperature and pH conditions, and in the presence of amelogenin, brushite transformed to monetite. Understanding the underlying mechanism of phase transformation and the unique structure of monetite derived from phase transformation provides us with insights that could lead to a new biomimetic approach to developing biomaterials for dental repair needs.

2. EXPERIMENTAL SECTION

2.1. Protein Expression and Purification

Recombinant porcine amelogenins (rP172 and rP148) were expressed in Escherichia coli strain BL21-codon plus (DE3-RP, Agilent Technologies, Inc., Santa Clara, CA) as previously described.(30-33) Protein purification was accomplished on a reverse phase C4 column (10 × 250 mm, 5 μm) mounted on a Varian Prostar HPLC system (ProStar/Dynamics6, version 6.41 Varian, Palo Alto, CA), using a linear gradient of 60% acetonitrile at a flow rate of 1.5 mL/min. Recombinant porcine amelogenin rP172 is an analogue of full-length native porcine P173, which has 173 amino acids, but rP172 lacks the N-terminal Met and a phosphate group on Ser16.(34) The recombinant rP148 lacks the hydrophilic C-terminal. The C-terminal (M149-D173) 25 amino acid residue peptide was synthesized at the Microchemical Core Laboratory at the University of Southern California, using a Pioneer peptide synthesizer (Applied Biosystems, Foster City, CA) following the N-Fmoc-l-amino acid pentafluorophyenyl ester/HOBt coupling method.(35)

2.2. Cleavage of rP172 by MMP-20

The recombinant human enamel proteinase Matrix Metalloproteinase 20 (rhMMP-20, Enzo Life Sciences, Farmingdale, NY) was mixed with 1.0 mg/mL rP172 at a mass ratio of 1:500 (0.002 μg/μL MMP-20, 5 mM $CaCl_2$ and 20 μM $ZnCl_2$ in 50 mM Tris-HCl, pH = 8.0) and then incubated at 37 °C for 18 h during cleavage. The protein mixture after cleavage was frozen at −20 °C for subsequent SDS-PAGE and crystallization experiments.

2.3. Electrophoresis

Sodium dodecyl sulfate–polyacrylamide gel electrophoresis (SDS–PAGE) was carried out with a 12% acrylamide gel to monitor the progress of amelogenin digestion. The gel was stained with Coomassie brilliant blue. Ten microliters of amelogenin cleavage product was loaded at a concentration of 1.0 mg/mL. The same volumes and concentrations of rP172 and rP148 were also

loaded as controls to identify the composition of amelogenin cleavage products. About 5 μL of Precision Plus Protein Kaleidoscope Standard (250 kDa, BIO-RAD, USA) was loaded as a marker.

2.4. Amelogenin rP172 Fluorescent Labeling

To observe the distribution of recombinant amelogenin rP172 on the crystal surfaces under fluorescence spectroscopy, rP172 was labeled with fluorescein isothiocyanate (FITC) as follows: FITC (1.25 μL of 1.0 mg/mL) was mixed with rP172 (62.5 μL 1.0 mg/mL) at a 1:50 ratio of FITC to protein at 37 °C in the dark for 1 h. Deionized water was used as a control in fluorescent labeling, with the same volume (62.5 μL) mixed with FITC (1.25 μL of 1.0 mg/mL) using the same procedure. The FITC-labeled solutions were then mixed with the solutions used in the synthesis of brushite crystals.

2.5. Brushite Synthesis with and without Amelogenin

Brushite crystals were synthesized following the previously published protocol with a slight modification.(36) KH_2PO_4–$CaCl_2$ solution containing rP172 was prepared by adding 62.5 μL of 1.0 mg/mL rP172 into a solution of 2.5 mL of KH_2PO_4(0.18 M) and 1.25 mL of $CaCl_2$ (0.4 M). Then, 2.5 mL of Na_2HPO_4 (0.02 M) was slowly titrated into the rP172-containing KH_2PO_4–$CaCl_2$ solution at room temperature, while the pH of the reaction solution was maintained at 5.5 by adding NaOH. The final concentration of rP172 in the mineralization solution was 0.1 mg/mL. The crystals were allowed to grow at room temperature for 5 days while being shaken. The deposited crystals were then separated from the solution using a centrifuge at 10 000 rpm for 10 min.

2.6. Sequential Washing of Brushite Crystals

Crystals were prepared for characterization with X-ray diffraction (XRD), fluorescent microscopy, atomic force microscopy (AFM), and Raman spectroscopy as follows: After centrifugation, the crystals were washed sequentially with deionized water (10 times) and phosphate buffer (pH 5.5, 1 M, 30 min), and the samples were centrifuged again at 10 000 rpm for 15 min after each wash process. Finally, the precipitates were lyophilized and stored at 4 °C for future characterizations. To observe the effect of the washing process, the products were also collected without any washing and after washing with only water. Parallel experiments with BSA (at the same final concentration of 0.1 mg/mL) or deionized water (containing FITC) were carried out under the same conditions for comparison. These are referred to as the BSA control group and water control group, respectively.

2.7. Fluorescence Spectroscopy

Fluorescence spectroscopy was performed using a PTI Quanta Master QM-4SE spectrofluorometer (PTI, Birmingham, NJ, USA). For all the samples, the fluorescent signal was excited at 435 nm, and the emission spectral peak was at 519 nm. The same samples were also characterized by confocal microscopy (Leica TCS SP5 confocal microscope).

2.8. X-ray Diffraction (XRD)

The lyophilized crystal powder samples were tightly pressed into SiO_2 diffraction plates 2 mm in height and 20 mm in diameter. The SiO_2 zero diffraction plates 30 × 30 × 2.5 mm (2sp) with Cavity 20 ID × 1.0 mm were purchased from MTI Corporation, USA. XRD patterns were recorded on a Rigaku diffractometer with Cu Kα radiation (λ = 1.542 Å) operating at 70 kV and 50 mA with a step size of 0.08°, at a scanning rate of 4°/min with a 2θ range from 5° to 65°.

2.9. Fourier Transform Infrared Spectroscopy (FTIR)

Transmittance infrared spectroscopy was carried out using lyophilized crystal samples/KBr tablets on a Spectrum GX FTIR (PerkinElmer, USA) in the region of 4000–400 cm^{-1} with a resolution of 2 cm^{-1}.

2.10. Thermal Gravity Analysis (TGA)

Two TGA experiments were conducted separately in this study. For Figure 4a, the fresh samples prepared with 0.1 mg/mL amelogenin (experimental group) and without protein (control group) were lyophilized and used. For TGA curves in Figure 5a, the samples prepared with 0.1 mg/mL amelogenin were tested after being kept in dry conditions at room temperature for three months. The samples weighed approximately 5 mg and were loaded into tin containers and tightly folded to remove air; the tin containers' weight was prebalanced. TGA was performed using TA Instruments Q5000 IR equipment. The temperature was kept at 25 °C for 10 min, then ramped to 1000 °C at a rate of 50 °C/min, and the sample weight loss during temperature ramping was recorded.

2.11. Scanning Electron Microscopy (SEM)

Scanning electron microscopy (SEM) was performed using a JEOL 7001-FEG microscope with an accelerating voltage of 10 kV. Sample powder was evenly distributed onto adhesive carbon tapes that were attached to aluminum mounts (12 mm in diameter, 10 mm in height) and then coated with 80/20 platinum/palladium before loading into the microscope.

2.12. Micro-Raman Spectroscopy

Samples were put onto glass coverslips in the form of powder. The Raman spectra were collected on single crystals from 100 to 4000 cm^{-1} under back scattering geometry by a LabRAM

ARAMIS confocal Raman microscope (HORIBA scientific, Japan), operated at a resolution of 2 cm^{-1} with an excitation wavelength of 532 nm and laser power of 2.5 mW. A ×60 objective with numerical aperture of 0.75 was used to focus the sample and collect spectra for 20 s. The experiment was repeated three times for each sample and results were averaged.

2.13. Atomic Force Microscopy (AFM)

A muscovite mica disc (9.9 mm in diameter; Ted Pella, Inc.) was freshly cleaved and used as a supporting surface. The mica surface was functionalized through treatment with 50 μL of poly-l-lysine solution (0.1% w/v, Ted Pella) for 5 min and then thoroughly rinsed with water and dried using a stream of nitrogen gas. The above-mentioned freshly prepared and lyophilized DCPD crystals washed with phosphate buffer were dispersed in PBS solution (Sigma-Aldrich) containing 10 mM phosphate and 154 mM NaCl at pH 7.4. Twenty microliters of this suspension was placed on the functionalized mica in 1 min. After allowing 10 min for thermal relaxation, time-lapse AFM images were continuously collected, first in PBS solution and later in water inside a fluid cell.

All in situ AFM images were captured in tapping mode at room temperature (23 °C) with a NanoScope 8 atomic force microscope (E scanner, Bruker) using silicon tips on silicon nitride cantilevers (HYDRA triangular lever, k = 0.088 N/m, tip radius <10 nm; resonance frequency 75 kHz in air; Applied Nanostructures, Inc.). The AFM cantilevers were treated with plasma to remove residual organic material from the surface before in situ imaging. The signal-to-noise ratio was maintained above 10. The scanning speed was 1–2 Hz. The amplitude set point was carefully tuned to minimize the average loading force (~50 pN) during imaging.

In order to identify whether the particles adsorbed on the step edges of the brushite (010) surface were protein or inorganic, force curves were collected on the crystal terraces as well as on

the single particles. The force curves collected on the particles showed multiple ruptures up to 21 nm extension, while the ones collected on the crystal terraces showed a single rupture. Force curves were collected in water with a constant approach and retraction velocity of 500 nm/s and a surface dwell time of 1 s. The spring constant of the cantilever was calibrated by deflection sensitivity and thermal fluctuation measurements.(37)

3. RESULTS AND DISCUSSION

3.1. Amelogenin Adsorption on Brushite Crystal Surfaces

Brushite crystals were synthesized in the absence and presence of amelogenin. Fluorescence microscopy (Figure 1) was used to examine the presence of amelogenin adsorbed on the brushite crystal surfaces, leading to morphological changes. The intensity of fluorescence without amelogenin (Figure 1a–c) was considerably weaker than the intensity with amelogenin (Figure 1d–f) under the same conditions.

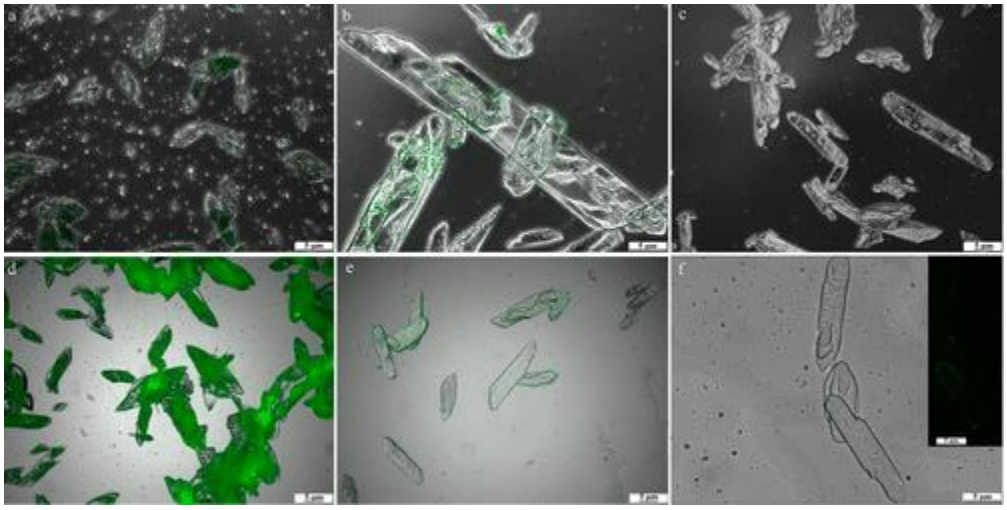

Figure 1. Fluorescent microscopy of brushite crystals: (a–c) control group without proteins: no wash, water wash and phosphate wash; (d–f) experimental group with 0.1 mg/mL amelogenin: no wash, water wash and phosphate wash; (inset) fluorescent microscopy of panel f.

Fluorescent microscopy of the water control group shows that, without amelogenin, the green fluorescence was weak (Figure 1a). The water wash process could remove most of the surface-adsorbed fluorescence (Figure 1b). After a phosphate buffer wash, there was no fluorescence left on the crystals (Figure 1c). This result demonstrates that FITC alone did not have a strong affinity to brushite crystals and was easily removed through the washing process.

Figure 1d shows there was a considerable fluorescent signal on the brushite crystal surface in the experimental group with amelogenin. After a water wash, most of the surface-adsorbed fluorescence was removed, but the remaining fluorescence could still clearly demarcate the shape of brushite crystals (Figure 1e). Compared to Figure 1b, in which the fluorescence was randomly distributed through the brushite crystal surface, the fluorescent signal in Figure 1e was clearly restricted and pronounced along the crystal edges, which gave a hint of locations of amelogenin adsorption. The subsequent phosphate buffer wash effectively removed most of the fluorescence, but the remaining green fluorescent light of FITC pointed out the locations where amelogenin adsorbed on the brushite crystal surface (inset in Figure 1f). Most of the fluorescence was apparent on the crystal edges, though a small amount presented at the step edges of the layered structure produced by amelogenin (Figure 1f). Brushite crystal morphology was affected by amelogenin: the rhombic crystal shape became less regular (Figure 1e), and the longitudinal edges were not sharp as in the water control group (Figure 1b). The green fluorescence left on the brushite after water and phosphate buffer washes in Figure 1 demonstrates that the affinity between amelogenin and brushite crystals was strong.

3.2. Amelogenin Adsorption Affects Brushite Crystal Morphology

Typically, brushite crystals have a platelet-like morphology with prominent (010) and lateral (h0l) faces.(38) Without additives, the growth of brushite was observed as the movement of atomically flat steps generated at complex dislocation on the (010) face.(39) This spiral growth usually results in the formation of a smooth crystal surface, as shown in Figure 2a.(38) In contrast, in situ AFM of the crystals shows that the surface roughness observed in the presence of adsorbed amelogenin was due to more sublayers on the brushite (010) surface (Figure 2b). In Figure 2c, a SEM image shows a side view of the layered structure induced by amelogenin adsorption on the brushite (010) surface. This morphological change was also revealed by confocal fluorescence microscopy (Supplementary Figure 1a) and SEM with higher magnification (Supplementary Figure 1b). Unlike amelogenin, bovine serum albumin (BSA), which was used as a control additive, did not affect brushite crystal morphology (Figure 2d). The BSA group showed a smooth (010) surface, like the control group in which no proteins were added (Figure 2a). Previously, it was reported that BSA had a tendency to be adsorbed on the crystal step edges in the presence of sodium bis(2-ethylhexyl) sulfosuccinate (AOT), leading to the growth of screw-like crystals.(40) BSA played an adsorption role to stabilize the structure. BSA itself cannot manipulate the brushite morphology.(41, 42)

Figure 3 shows the AFM images of brushite crystals prepared without and with amelogenin. In Figure 3a, which represents the control group without addition of amelogenin, the brushite (010) surface was very smooth with a series of terraces. When DCPD was synthesized in the presence of amelogenin, the surface was rougher, and a number of round particles were observed at the crystal edges (Figure 3b). After a phosphate buffer wash, the control brushite crystal surface did not

change significantly (Figure 3c), but the morphology of some adsorbed amelogenin particles became string-like (Figure 3d).

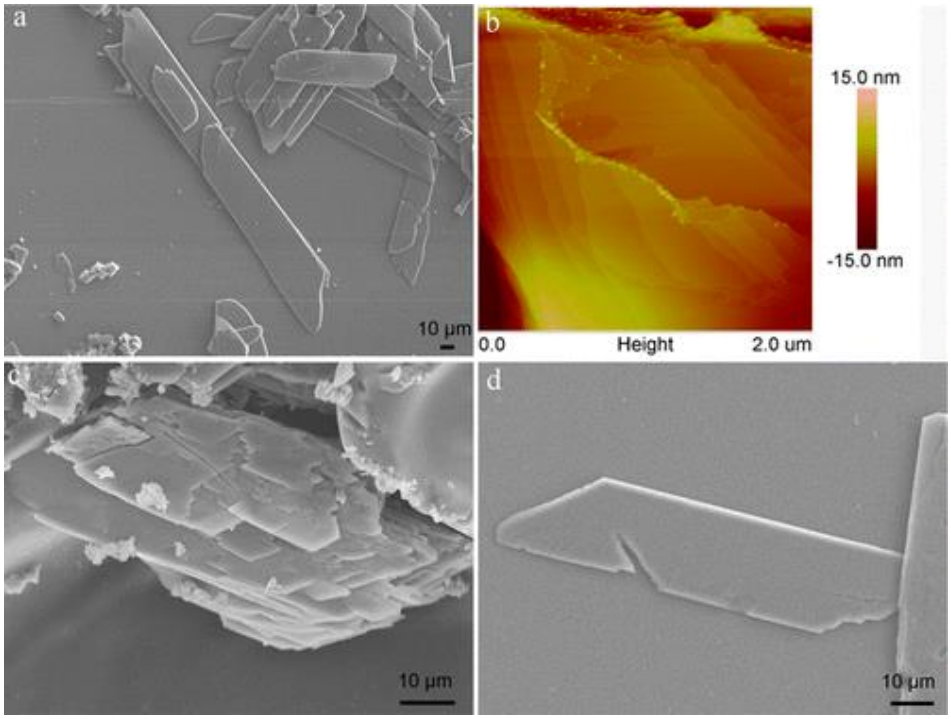

Figure 2. (a) SEM image of brushite crystals formed without proteins; (b) in situ AFM; and (c) SEM image of layered structure on brushite (010) surface formed with 0.1 mg/mL amelogenin; (d) SEM image of brushite crystals formed with 0.1 mg/mL BSA.

Force measurement was performed to differentiate the phases of particles from DCPD grown with amelogenin after a water wash. The interactions between particles, crystal terraces, and the Si tip were measured by engaging the tip toward the target and dwelling for 1 s. The retraction curves are shown in Figure 3e. The shapes of the force curves were quite different in different locations: on the crystal terrace, we only observed single rupture events, while on the particles on the edges we found multiple rupture events. Multiple rupture force curves are an indication of interaction between the silicon tip and stretchable macromolecules such as proteins.(43, 44) Complete rupture occurred when the separation between the tip and the DCPD face was up to 21 nm.

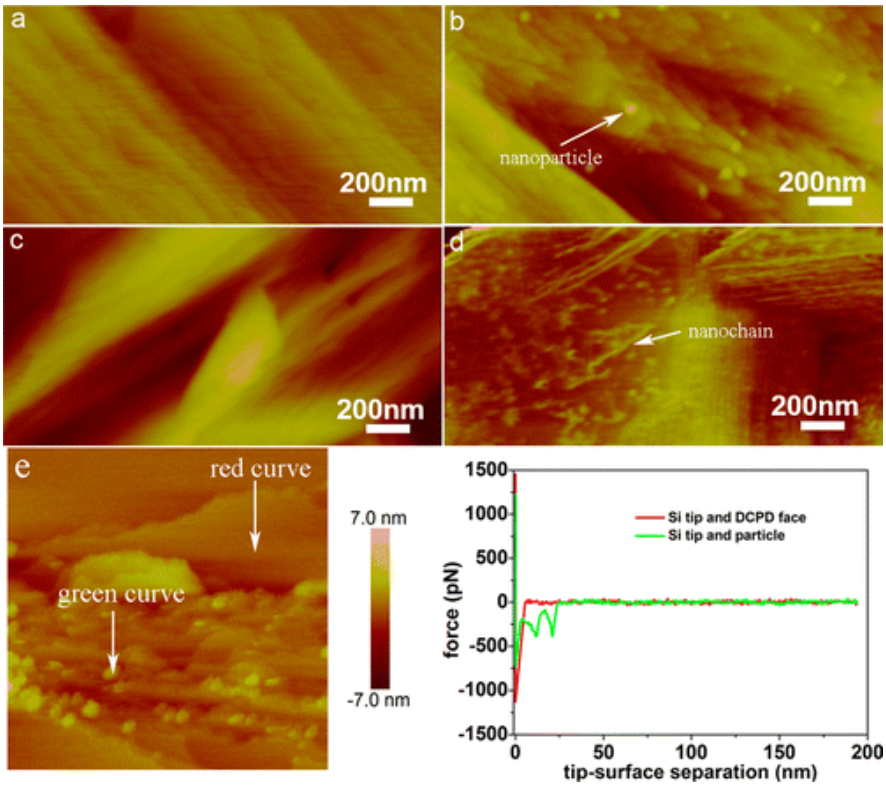

Figure 3. AFM images of lyophilized brushite crystals (a) control, after water wash; (b) 0.1 mg/mL amelogenin, after water wash; (c) control, after phosphate buffer wash; and (d) 0.1 mg/mL amelogenin, after phosphate buffer wash. (e) Image and corresponding force curves of amelogenin adsorbed on brushite crystal, after water wash (red curve from plain surface on the image; green curve from nanoparticle on the image). Force on crystal: 826.2 ± 392.2 pN (5 curves); on particle: 223.5 ± 128.8 pN (13 curves).

Although it could not be definitively ascertained whether the final rupture occurred at the particle–DCPD interface or the particle–tip interface, an extension of 21 nm is relatively large compared to the height of a particle, which is only 2–3 nm. This indicates that a chain-like structure is stretching from the surface of the particle, so this large extension should be attributed to the behavior of the protein when it is being pulled between the tip and the DCPD surface. Similar multiple ruptures have been observed in the force curves obtained by pulling collagen out

of a hydroxyapatite (100) face,(43) as well as in the force curves obtained by pulling enamel matrix proteins out of enamel crystals.(44)

On the basis of these observations, we suggest that amelogenin adsorption plays a critical role in changing brushite crystal morphology. According to the classical theory of crystallization the morphology of a crystal is determined by the relative growth rates of its individual faces. When additives are adsorbed preferentially onto a certain face, its relative growth rate decreases and that face is expressed more in the final morphology.(45) In aqueous solution, the dominant (010) face of brushite crystal is composed of bilayers of structural water molecules, and lateral faces express a mixed ionic nature with exposed calcium and phosphate ions.(46) During brushite crystal growth in the presence of amelogenin, the specific affinity of the amelogenin toward the calcium ions as well as the crystal water molecules might change the growth mechanism from spiral growth to surface nucleation.(39) Spiral growth has been stated as the most dominant mechanism of brushite crystal growth under additive-free conditions. When amelogenin is added to the reaction medium, the adsorption of proteins could dramatically increase the solid–liquid interfacial energy of brushite, which would delay the formation of active spiral step sources. In this case, the growth of the brushite crystal may proceed via surface nucleation to generate new growth sites when the driving force (supersaturation) is high enough. As a result, the brushite morphology is affected by the interaction of amelogenin with the crystal surface. Similar findings were also reported in a study of additive interactions with brushite, in which the macromolecules and molecules that altered its structure were specifically adsorbed on the dominant (010) face.(47)

3.3. Amelogenin Promotes Brushite–Monetite Phase Transformation

The amelogenin adsorption on brushite was further confirmed by TGA studies. Unwashed brushite crystals prepared with and without amelogenin were taken for TGA characterization. The obtained TGA curve (Figure 4a) shows that as the temperature increased, there were three stages of weight loss in the control group (red curve). The first stage, a rapid drop between 150 and 200 °C, with a weight loss of 20%, represents the dehydration of brushite to form monetite ($CaHPO_4 \cdot 2H_2O \rightarrow CaHPO_4 + 2H_2O$, $\Delta m = 21\%$).(14) The second and third stages, with a weight loss of ∼6% in total as the temperature ramped up from 200 to 500 °C, correspond to the thermal decomposition of anhydrous monetite ($CaHPO_4$) to form γ-$Ca_2P_2O_7$ ($2CaHPO_4 \rightarrow$ γ-$Ca_2P_2O_7 + H_2O$, $\Delta m = 6.6\%$).(48) In the experimental group, where 0.1 mg/mL amelogenin was added, the curve (Figure 4a, black curve) also shows three stages of weight loss. As expected, the first stage with 21% weight loss represents transformation of brushite to monetite. The total weight loss in the second and third stages is ca. 21%, which is higher than observed in the control group (6%). The extra weight loss demonstrates the presence of amelogenin on the crystal surface, which is consistent with the observations in Figure 1d and Figure 3. In addition, we cannot rule out the possibility that amelogenin may also be occluded during crystal growth, which has been previously reported in the case of calcite.(57) Further studies are needed to confirm the exact location and amount of amelogenin in the brushite crystals.

In addition, it is worth noting that the presence of amelogenin made the dehydration of brushite occur earlier (or faster) in both the first and the second stages. In the first stage, brushite formed with amelogenin lost its crystalline water at a lower temperature (195 °C) than in the control group (210 °C). In the second stage, water loss in the amelogenin group happened at 440 °C, while in the control group it occurred at 455 °C. We therefore deduced that amelogenin

destabilizes the crystalline water layer in brushite and promotes phase transformation of Ca–P crystals from a less stable phase (brushite) to more stable phases during a temperature rise. The destabilization effect of amelogenin on the crystal water in brushite was further revealed by the micro-Raman spectroscopy studies.

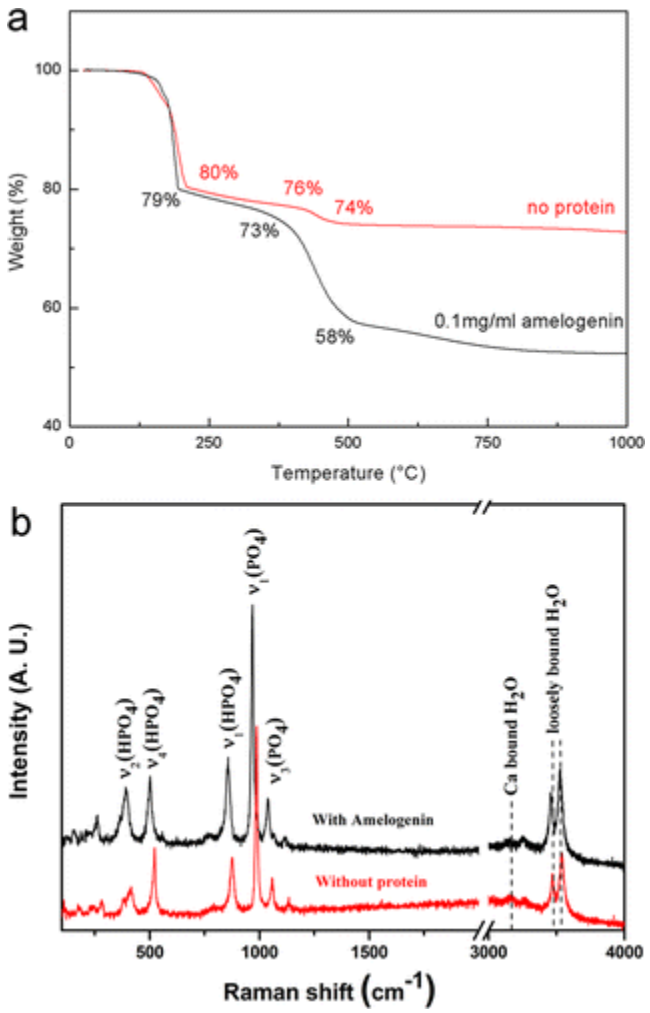

Figure 4. (a) TGA curves of lyophilized brushite crystals grown with no protein (red curve) or 0.1 mg/mL amelogenin (black curve); (b) Raman spectra of brushite crystals grown with no protein (red curve), after water wash or 0.1 mg/mL amelogenin (black curve), after water wash.

As shown in Figure 4b, the Raman spectrum of brushite prepared without amelogenin (red curve in Figure 4b) shows the presence of nonequivalent water molecules, namely, Ca-bound H_2O and

loosely bound H_2O (Figure 4b).(49, 50) The water layers formed by Ca-bound H_2O are highly ordered and comparably stable, and therefore can be considered as part of the brushite crystal structure, whereas the loosely bound H_2O layers exhibit no in-plane order, but rather are only layered in the direction perpendicular to [010].(51) When the Raman spectrum of brushite crystals prepared with amelogenin (black curve in Figure 4b) was examined, it was found that the characteristic band for Ca-bound H_2O was reduced, whereas the band for loosely bound H_2O was increased. Specifically, when compared to the Raman spectrum in the control group (without amelogenin), the intensity ratio between the characteristic bands for loosely bound H_2O (at 3475 cm^{-1}) and $\nu_1(PO_4)$ (at 986 cm^{-1}) was increased from 0.21 to 0.27 in the experimental group (with amelogenin). These results indicate that the Ca-bound H_2O in the brushite crystals tends to be destabilized to form loosely bound H_2O due to the presence of amelogenin in the system.

In a separate series of experiments, when crystals were left at room temperature for three months in the dry state, amelogenin adsorbed on a brushite surface promoted crystal phase transformation from brushite to monetite. The TGA analysis results (Figure 5a) of crystals after setting for three months at room temperature show that, during temperature ramping, the weight loss behavior of crystals formed with amelogenin was quite different than those without amelogenin. As shown in Table 1, analysis by XRD revealed that phase transformation processes varied between groups with different washing procedures. On the basis of the main peak intensity, all of the brushite crystals (JCPDS 72-1240) grown with amelogenin and without washing transformed into monetite (JCPDS 71-1759, Figure 5b, blue line); after washing with water, on the basis of the calculation of the highest peaks of brushite and monetite, about 3/5 of the brushite crystals transformed into monetite (Figure 5b, red line), whereas in those washed with phosphate

buffer, thereby removing almost all of the surface-adsorbed amelogenin, no crystal phase transformation occurred (Figure 5b, black line).

Table 1. Brushite Phase Transformation to Monetite in the Absence and Presence of Amelogenin under Different Washing Conditions

	without wash	***water wash***	***phosphate buffer wash***
control, no protein, fresh	*brushite*	*brushite*	*brushite*
amelogenin, fresh	*brushite*	*brushite*	*brushite*
amelogenin, kept for three months at room temperature in dry state	*monetite*	*3/5 monetite, 2/5 brushite*	*brushite*

Ren, Dongni; Ruan, Qichao; Tao, Jinhui; Lo, Jonathan; Nutt, Steven; Moradian-Oldak, Janet, **"Amelogenin affects brushite crystal morphology and promotes its phase transformation to monetite"** Crystal Growth & Design Aug 16 [9] 4981-90 (2016) DOI: **10.1021/acs.cgd.6b00569**

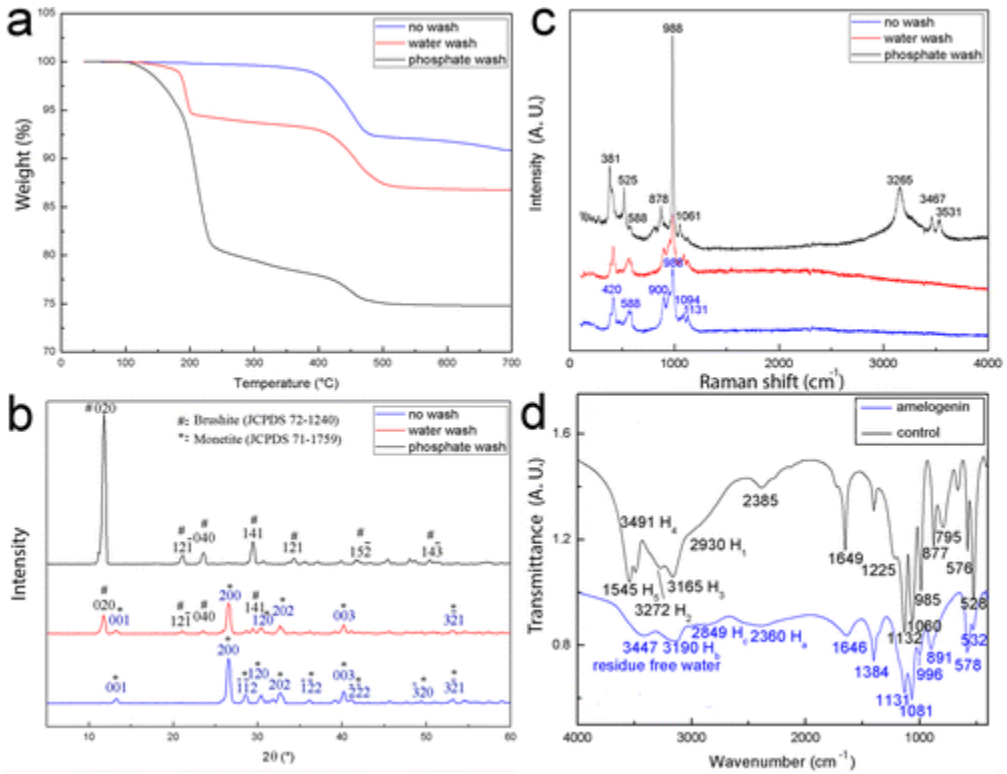

Figure 5. (a) TGA, (b) XRD, and (c) micro-Raman analyses of the samples prepared in the experimental group with 0.1 mg/mL rP172 after being kept in dry conditions at room temperature for three months: blue curve, without wash; red curve, water wash; black curve, phosphate buffer wash. In panel b, diffraction peaks of brushite (#) and monetite (*) are labeled according to the standard patterns of JCPDS 72-1240 and JCPDS 71–1759. (d) Transmittance FTIR of lyophilized crystal samples formed with (blue curve) or without amelogenin (black curve), kept in dry conditions at room temperature for three months.

The micro-Raman (Figure 5c) analysis of crystals grown with amelogenin supported the finding that amelogenin promotes brushite-monetite phase transformation in the dry state. The peaks in the blue curve (no wash) in Figure 5c match well with reported monetite peaks, while the peaks in the black curve (phosphate wash) in Figure 5c match well with the brushite peaks.(52) This also demonstrates that surface-adsorbed amelogenin can promote phase transformation. The red curve inFigure 5c contains peaks from both brushite and monetite, from which we can deduce there might be a small amount of amelogenin remaining on the brushite crystal surface after a water wash, and this could also promote phase transformation.

Ren, Dongni; Ruan, Qichao; Tao, Jinhui; Lo, Jonathan; Nutt, Steven; Moradian-Oldak, Janet, **"Amelogenin affects brushite crystal morphology and promotes its phase transformation to monetite"** Crystal Growth & Design Aug 16 [9] 4981-90 (2016) DOI: **10.1021/acs.cgd.6b00569**

The brushite–monetite solid-state phase transformation was also demonstrated by transmittance FTIR at room temperature. The crystals formed with or without amelogenin in solution were selected (without washing after mineralization and drying at room temperature for more than three months). The black curve shown in Figure 5d is the crystal formed without amelogenin. The peaks of this curve match the brushite peaks reported in the literature, which means there was no phase transformation. The blue curve in Figure 5d is the crystal formed with amelogenin, and the peaks in this curve match the peaks reported in the literature for monetite, showing that a solid-state phase transformation occurred and was mediated by amelogenin.(42, 53) A 3447 cm^{-1} broad peak in the blue curve in Figure 5d might represent the residue-free water and provides a hint that amelogenin mediates the solid-state phase transformation through crystalline water.

Brushite belongs to a non-centrosymmetric, monoclinic space group *Ia* (C_4^s) with $Z = 4$. The parameters of each unit cell are $a = 5.812$, $b = 15.180$, $c = 6.239$ Å, $\beta = 116.42°$.(14, 54, 55) Brushite crystal has a layered structure in which the layers are held together by crystalline water molecules via hydrogen bonds. It has been previously reported that acidic amino acids like Asp and Glu could be adsorbed on a brushite crystal surface and promote its phase transformation to HAp by reducing the interfacial energy barrier.(56) Amelogenin can adsorb onto brushite crystal surfaces through its C-terminus, which contains several acidic amino acids including Asp and Glu.(39) Our TGA results support the notion that amelogenin can promote brushite phase transformation by destabilizing crystalline water through interaction with the acidic amino acids of the amelogenin C-terminus. Supporting this view, TGA and XRD results also show multistage crystalline water loss from the brushite crystals. We suggest that the presence of amelogenin on a

brushite surface can promote phase transformation, and this effect is related to the rate of crystalline water loss. Amelogenin-promoted brushite-monetite crystal phase transformation can happen rapidly at a high temperature (TGA temperature ramping) or more slowly at a low temperature (room temperature, 3 months).

SEM images show significant differences in monetite crystal morphology between the control and the experimental groups after they were left dry for several weeks at room temperature. In the control (Figure 6a) without protein, the crystal surface was smooth. In contrast, in the experimental group (Figure 6b) with amelogenin, not only was the crystal phase transformation more rapid, the crystal morphology was affected. Small, monetite platelets with a high aspect ratio were observed, and the thickness of the crystals was around 100 nm (Figure 6c). Considering the important role of monetite as a precursor to HAp, the formation of this interlocking structure of monetite may provide new inspiration to develop biomimetic HAp materials.

Ren, Dongni; Ruan, Qichao; Tao, Jinhui; Lo, Jonathan; Nutt, Steven; Moradian-Oldak, Janet, **"Amelogenin affects brushite crystal morphology and promotes its phase transformation to monetite"** Crystal Growth & Design Aug 16 [9] 4981-90 (2016) DOI: **10.1021/acs.cgd.6b00569**

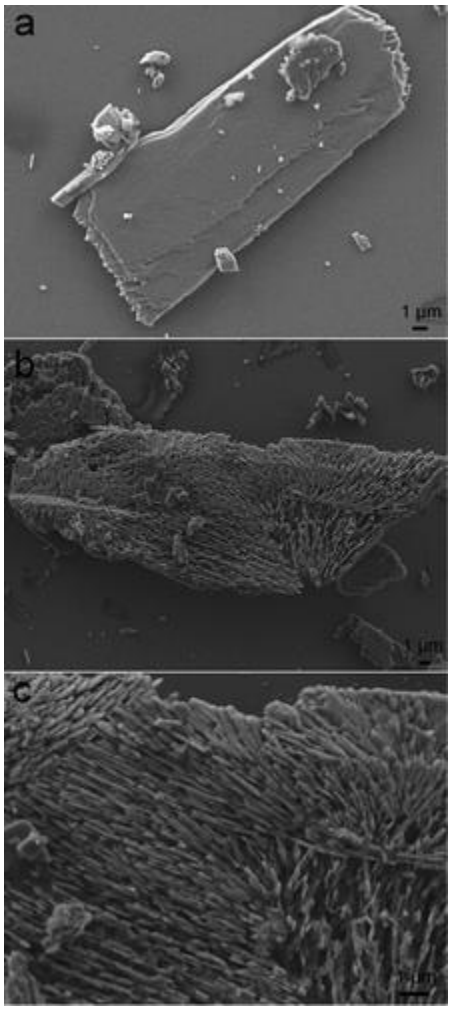

Figure 6. SEM images of monetite transformed from brushite in a dry state: (a) control, no protein; (b) 0.1 mg/mL amelogenin; (c) higher magnification of the monetite crystal in panel b with interlocked platelet morphology.

3.4. Amelogenin–Brushite Interaction Occurs via the C-Terminus

In order to demonstrate its involvement in amelogenin–brushite interactions, the hydrophilic C-terminal segment of amelogenin was cleaved by MMP-20 prior to brushite crystal growth. There are six acidic amino acids [Asp (D) and Glu (E), marked in red] in the amelogenin C-terminus, and its isoelectric point is relatively low (pI = 4.05) (Figure 7a).(57) After 18 h incubation with MMP-20 at 37 °C, amelogenin rP172 was cleaved by MMP-20, removing its C-terminus and producing

digestion products that have been previously identified.(58) The digestion products of amelogenin produced four bands when examined via SDS-PAGE: a very faint band at around 25 kDa indicating the remaining uncleaved rP172, and three new bands at around 20 kDa, 13 kDa, and 11 kDa. The 20 kDa band, which appeared at the same height as control rP148 (2–148), was the main cleavage product of rP172. The 13 kDa protein might be a subsequent cleavage product, 46–148 (Figure 7b) and the 11 kDa protein is the 64–148 product.(59-61) Adding a mixture of amelogenin and MMP-20 proteolytic products to brushite did not cause any morphological changes (Figure 7c). These experiments demonstrate that the C-terminal acidic amino acids are essential to the binding between full-length amelogenin and brushite crystals. We have previously reported that the action of MMP-20 on amelogenin also reduces amelogenin–apatite binding.(33)

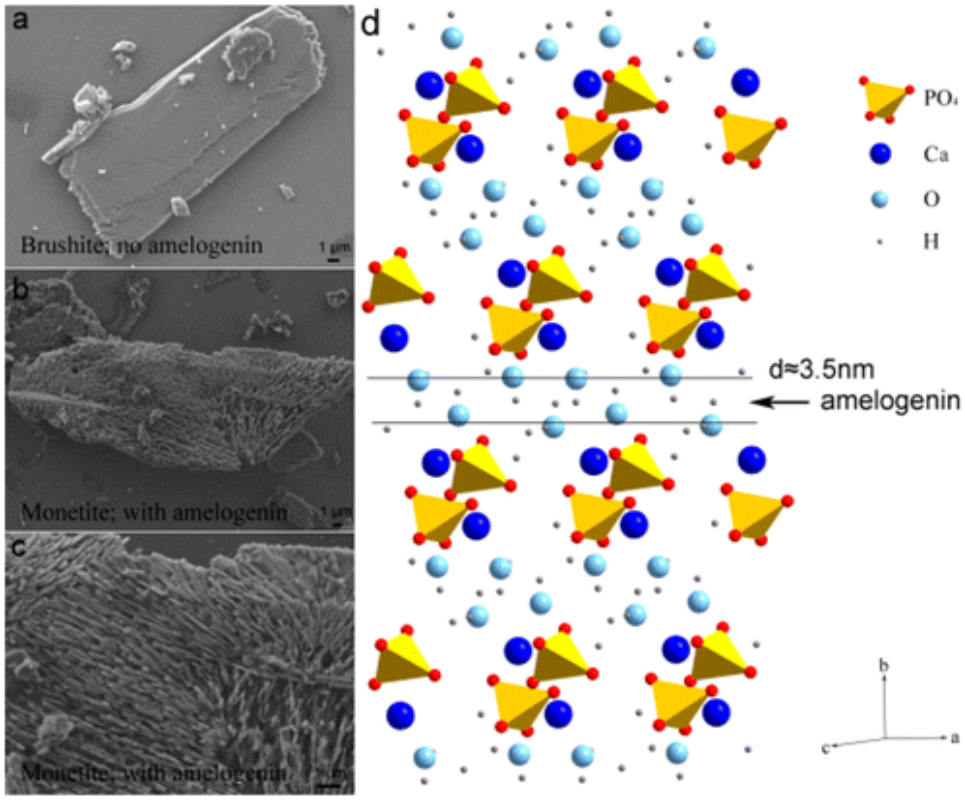

Figure 7. (a) The sequence of recombinant full-length amelogenin rP172,(56) with the 25 amino acids of the C-terminal domain underlined. (b) SDS-PAGE after amelogenin was cleaved by

Ren, Dongni; Ruan, Qichao; Tao, Jinhui; Lo, Jonathan; Nutt, Steven; Moradian-Oldak, Janet, **"Amelogenin affects brushite crystal morphology and promotes its phase transformation to monetite"** Crystal Growth & Design Aug 16 [9] 4981-90 (2016) DOI: **10.1021/acs.cgd.6b00569**

MMP-20 (1:500). The bands have been identified as I: rP172, II: 20k or 2-148, III: 13K or 46-148 and IV: 11k or 63-148;(57) (c) SEM image of brushite crystals formed with the proteolytic mixture of cleaved amelogenins.

Remarkably, when the C-terminal 25-mer peptide of amelogenin was used in brushite *in vitro* mineralization, no effect on the morphology was observed. The micro-Raman peaks of the crystals grown in the presence of the 25-mer showed a pattern similar to the control groups (no wash, water wash, and phosphate wash); they all matched well with peaks reported in the literature for brushite, with a small blue shift (Supplementary Figure 2), which means that the C-terminal residue alone is not enough to trigger the solid-state phase transformation of brushite.(51) The hydrophobic portion of full-length amelogenin might act as a stabilizer and help the hydrophilic C-terminus to interact with brushite crystalline water, thus pulling the water out of the crystals. This might also provide a potential insight into the function of amelogenin during enamel formation.

Keith et al. reported that metastable oligomers of amelogenin were present in solution at pH = 5.5 and that the C-terminus of amelogenin was exposed at the surface.(62) The hydrodynamic radius (R_H) of such oligomers ranged between 4 and 7.5 nm, depending on protein concentration; the R_H decreased along with protein concentration. Specifically, the average R_H of the major amelogenin oligomers decreased with increasing dilution at 22 °C from around 7.5 nm at 10 mg/mL to around 4.0 nm at 0.5 mg/mL. The amelogenin oligomers would provide more surface area for binding to the crystals than amelogenin nanospheres.(62) In the current study, the amelogenin concentration in the mineralization solution is 0.1 mg/mL, much lower than the protein concentration reported in literature; thus, we deduce that the R_H of the amelogenin oligomer in our experiment might be smaller than 4 nm, which may fit in the space (around 3.5 nm) between the two crystalline water layers in brushite crystals (Figure 8).

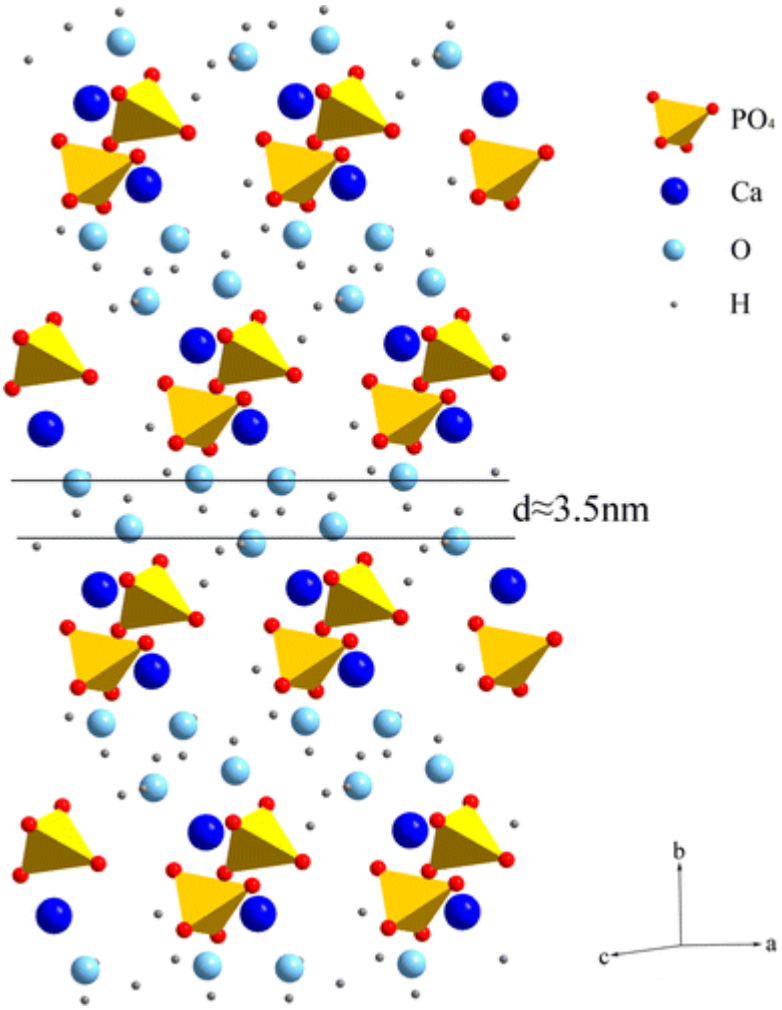

Figure 8. Brushite crystal structure showing spacing between crystalline water layers fits with the RH of amelogenin oligomer (figure generated by Diamond Version 4.0.5).(53)

An electronic adherence might exist between the negatively charged C-terminal segment and brushite Ca^{2+} ions at pH 5.5, the condition under which crystallization occurred in our experiments. Amelogenin would therefore have a tendency to adsorb on the brushite surface via the Ca ions and compete against the Ca-bonding crystalline water. Thus, the affinity between the Ca ions and H_2O molecules would be weakened, causing the crystalline water in brushite to be lost when the dry material was stored at room temperature. This water loss could then trigger a phase transformation to monetite. In this phase transformation, amelogenin acted as a catalyst that

promoted the transformation of less stable brushite to a more stable monetite. We therefore suggest that this unusual function of amelogenin during the brushite–monetite phase transformation was due to its indirect reaction with crystalline water as a competition coordinator to Ca ions. The two water molecules in brushite are not identical: it was reported that one water molecule has nearly linear hydrogen, and these hydrogen bonds between layers are the weak points that break as the water molecules leave the crystals during phase transformation.(14, 55, 63) It is also reasonable to conclude that amelogenin affects the layered structure of brushite (010) face due to its competitive coordination against crystalline water, causing destruction of the laminated structure that had been stabilized by the hydrogen bonds in the crystalline water molecules.

4. CONCLUSIONS

We demonstrate that amelogenin adsorbed onto a brushite surface affected crystal morphology and caused the formation of layered structure on the brushite (010) face. Amelogenin promoted the phase transformation of calcium phosphate crystals from its less stable phase of brushite to a more stable state of monetite at room temperature. We suggest that amelogenin, due to its negatively charged C-terminus, can penetrate through the crystalline water layers in brushite and form strong bonds with the positively charged Ca ions, as a competitive coordination against the Ca-bonding crystalline water. This binding weakens the bonds between Ca ions and H_2O molecules, leading to the extraction of crystalline water from the crystals. We found that the newly grown layers caused by the addition of amelogenin continued developing even after the brushite–monetite phase transformation. Taken together, these studies provide new insights into a possible biomimetic approach to generating enamel repair material.

Ren, Dongni; Ruan, Qichao; Tao, Jinhui; Lo, Jonathan; Nutt, Steven; Moradian-Oldak, Janet, **"Amelogenin affects brushite crystal morphology and promotes its phase transformation to monetite"** Crystal Growth & Design Aug 16 [9] 4981-90 (2016) DOI: **10.1021/acs.cgd.6b00569**

Associated Content: The Supporting Information is available free of charge on the ACS Publications website at DOI: 10.1021/acs.cgd.6b00569.

Supplementary Figure 1. (a) Confocal microscopy and (b) SEM with higher magnification showing the layered structure formed on the brushite (010) surface in the presence of amelogenin. Supplementary Figure 2. Micro-Raman spectra of lyophilized crystal samples of control groups (no wash, water wash, and phosphate buffer wash) and the experimental group with amelogenin C-terminal 25-mer peptide. The samples were kept in a dry state at room temperature for three months before Raman testing (PDF)

Notes: The authors declare no competing financial interest.

Acknowledgements: This research was supported by NIH-NIDCR Grants DE-013414 and DE-020099. The authors would like to thank the Center for Electron Microscopy and Microanalysis (CEMMA) at USC for electron microscopy. The AFM and Raman measurements were performed at Pacific Northwest National Laboratory, which is a multiprogram national laboratory operated by Battelle for the US DOE under Contract DE-AC05-76RL01830. Karthik Balakrishna Chandrababu and Saumya Prajapati contributed to the protein preparation in this work. We thank Yunpeng Zhang for his help with the TGA and FTIR experiments.

References:

1. Johansen, E. *J. Dent. Res.* **1964**, 43, 1007– 1020, DOI: 10.1177/00220345640430060201
2. Habelitz, S.; Marshall, S. J.; Marshall, G. W.; Balooch, M. *J. Struct. Biol.* **2001**, 135, 294–301, DOI: 10.1006/jsbi.2001.4409
3. Marshall, G.; Balooch, M.; Gallagher, R.; Gansky, S.; Marshall, S. *J. Biomed. Mater. Res.* **2001**, 54, 87– 95, DOI: 10.1002/1097-4636(200101)54:1<87::AID-JBM10>3.0.CO;2-Z
4. Habelitz, S.; Marshall, S.; Marshall, G.; Balooch, M. *Arch. Oral Biol.* **2001**, 46, 173–183, DOI: 10.1016/S0003-9969(00)00089-3

5. Popowics, T.; Rensberger, J.; Herring, S. *Arch. Oral Biol.* **2004**, 49, 595– 605, DOI: 10.1016/j.archoralbio.2004.01.016
6. He, L. H.; Swain, M. V. *J. Mech Behav. Biomed.* **2008**, 1, 18– 29, DOI: 10.1016/j.jmbbm.2007.05.001
7. Bartlett, J. D.; Ganss, B.; Goldberg, M.; Moradian-Oldak, J.; Paine, M. L.; Snead, M. L.; Wen, X.; White, S. N.; Zhou, Y. L. *Curr. Top. Dev. Biol.* **2006**, 74, 57– 115, DOI: 10.1016/S0070-2153(06)74003-0
8. Gibson, C.W.; Yuan, Z.A.; Hall, B.; Longenecker, G.; Chen, E.; Thyagarajan, T.; Sreenath, T.; Wright, J. T.; Decker, S.; Piddington, R.*J. Biol. Chem.* **2001**, 276, 31871– 31875, DOI: 10.1074/jbc.M104624200
9. Wright, J.; Hart, P.; Aldred, M.; Seow, K.; Crawford, P.; Hong, S.; Gibson, C.; Hart, T. *Co nnect. Tissue Res.* **2003**, 44, 72– 78, DOI: 10.1080/03008200390152124
10. Sun, Z.; Fan, D.; Fan, Y.; Du, C.; Moradian-Oldak, J. *J. Dent. Res.* **2008**, 87, 1133– 1137, DOI: 10.1177/154405910808701212
11. Iijima, M.; Moradian-Oldak, J. *J.Mater.Chem.* **2004**, 14, 2189– 2199, DOI: 10.1039/b401961j
12. Beniash, E.; Simmer, J. P.; Margolis, H. C. *J. Struct. Biol.* **2005**, 149, 182– 190, DOI: 10.1016/j.jsb.2004.11.001
13. Elliott, J. C. *Structure and Chemistry of the Apatites and Other Calcium Orthophosphates*; Elsevier: Amsterdam, **2013**; Vol. 18.
14. Dosen, A.; Giese, R. F. *Am. Mineral.* **2011**, 96, 368– 373, DOI: 10.2138/am.2011.3544
15. Cama, G.; Barberis, F.; Capurro, M.; Di Silvio, L.; Deb, S. *Mater. Chem. Phys.* **2011**, 130, 1139– 1145, DOI: 10.1016/j.matchemphys.2011.08.047
16. Margolis, H.; Moreno, E. *Caries Res.* **1985**, 19, 22– 35, DOI: 10.1159/000260826
17. Shellis, R.; Heywood, B.; Wahab, F. *Caries Res.* **1997**, 31, 71– 77, DOI: 10.1159/000262377
18. Bernard, R. Process for the Preparation of Brushite Crystals, 3,679,360, **1972**.
19. Young, A. M.; Ng, P. Y. J.; Gbureck, U.; Nazhat, S. N.; Barralet, J. E.; Hofmann, M. P. *Acta Biomater.* **2008**, 4, 1081– 1088, DOI: 10.1016/j.actbio.2007.12.009
20. Tamimi, F.; Sheikh, Z.; Barralet, J. *Acta Biomater.* **2012**, 8, 474– 487, DOI: 10.1016/j.actbio.2011.08.005
21. Roop Kumar, R.; Wang, M. *Mater. Lett.* **2001**, 49, 15– 19, DOI: 10.1016/S0167-577X(00)00333-5
22. Biemond, J. E.; Eufrásio, T. S.; Hannink, G.; Verdonschot, N.; Buma, P. *J. Mater. Sci.: Mater. Med.* **2011**, 22, 917– 925, DOI: 10.1007/s10856-011-4256-0
23. Hsu, Y.-S.; Chang, E.; Liu, H.-S. *Ceram. Int.* **1998**, 24, 249– 254, DOI: 10.1016/S0272-8842(96)00056-9
24. He, W.-X.; Nik, S. M.; Andersson, M. *Cryst. Growth Des.* **2015**, 15, 5– 9, DOI: 10.1021/cg5016862
25. Furuichi, K.; Oaki, Y.; Imai, H. *Chem. Mater.* **2006**, 18, 229– 234, DOI: 10.1021/cm052213z
26. Ma, M.-G.; Zhu, Y.-J.; Chang, J. *J. Phys. Chem. B* **2006**, 110, 14226– 14230, DOI: 10.1021/jp061738r

27. Zou, Z.; Liu, X.; Chen, L.; Lin, K.; Chang, J. *J. Mater. Chem.* **2012**, 22, 22637– 22641, DOI: 10.1039/c2jm35430f
28. Liu, X.; Lin, K.; Wu, C.; Wang, Y.; Zou, Z.; Chang, J. *Small* **2014**, 10, 152– 159, DOI: 10.1002/smll.201301633
29. Ruan, Q.; Liberman, D.; Zhang, Y.; Ren, D.; Zhang, Y.; Nutt, S. R.; Moradian-Oldak, J. *ACS Biomater. Sci. Eng.* **2016**, 2, 1049– 1058,DOI: 10.1021/acsbiomaterials.6b00164
30. Hu, C.-C.; Bartlett, J.; Zhang, C.; Qian, Q.; Ryu, O.; Simmer, J. *J. Dent. Res.* **1996**, 75, 1735– 1741, DOI: 10.1177/00220345960750100501
31. Ryu, O.; Fincham, A.; Hu, C.-C.; Zhang, C.; Qian, Q.; Bartlett, J.; Simmer, J. *J. Dent. Res.* **1999**, 78, 743– 750, DOI: 10.1177/00220345990780030601
32. Ruan, Q.; Zhang, Y.; Yang, X.; Nutt, S.; Moradian-Oldak, J. *Acta Biomater.* **2013**, 9, 7289– 7297, DOI: 10.1016/j.actbio.2013.04.004
33. Sun, Z.; Ahsan, M. M.; Wang, H.; Du, C.; Abbott, C.; Moradian-Oldak, J. *Eur. J. Oral Sci.* **2006**, 114, 59– 63, DOI: 10.1111/j.1600-0722.2006.00296.x
34. Fincham, A. G.; Moradian-Oldak, J. *Biochem. Biophys. Res. Commun.* **1993**, 197, 248– 255, DOI: 10.1006/bbrc.1993.2468
35. Lokappa, S. B.; Chandrababu, K. B.; Moradian-Oldak, J. *Biochem. Biophys. Res. Commun.* **2015**, 464, 956– 961, DOI: 10.1016/j.bbrc.2015.07.082
36. Marshall, R. W.; Nancollas, G. H. *J. Phys. Chem.* **1969**, 73, 3838– 3844, DOI: 10.1021/j100845a045
37. Hutter, J. L.; Bechhoefer, J. *Rev. Sci. Instrum.* **1993**, 64, 1868– 1873, DOI: 10.1063/1.1143970
38. Ucar, S.; Bjørnøy, S. H.; Bassett, D. C.; Strand, B. L.; Sikorski, P.; Andreassen, J.-P. *Cryst. Growth Des.* **2015**, 15, 5397– 5405, DOI: 10.1021/acs.cgd.5b01032
39. Wu, S.; Zhai, H.; Zhang, W.; Wang, L. *Cryst. Growth Des.* **2015**, 15, 4490– 4497, DOI: 10.1021/acs.cgd.5b00754
40. Quan, Y.; Zhai, H.; Zhang, Z.; Xu, X.; Tang, R. *CrystEngComm* **2012**, 14, 7184– 7188, DOI: 10.1039/c2ce25805f
41. Xie, J.; Riley, C.; Chittur, K. *J. Biomed. Mater. Res.* **2001**, 57, 357– 365, DOI: 10.1002/1097-4636(20011205)57:3<357::AID-JBM1178>3.0.CO;2-1
42. Xie, J.; Riley, C.; Kumar, M.; Chittur, K. *Biomaterials* **2002**, 23, 3609– 3616, DOI: 10.1016/S0142-9612(02)00090-X
43. Tao, J.; Battle, K. C.; Pan, H.; Salter, E. A.; Chien, Y.-C.; Wierzbicki, A.; De Yoreo, J. J. *Proc. Natl. Acad. Sci. U. S. A.* **2015**, 112, 326–331, DOI: 10.1073/pnas.1404481112
44. Prajapati, S.; Tao, J.; Ruan, Q.; De Yoreo, J. J.; Moradian-Oldak, J. *Biomaterials* **2016**, 75, 260– 270, DOI: 10.1016/j.biomaterials.2015.10.031
45. Addadi, L.; Weiner, S. *Proc. Natl. Acad. Sci. U. S. A.* **1985**, 82, 4110– 4114, DOI: 10.1073/pnas.82.12.4110
46. Hanein, D.; Geiger, B.; Addadi, L. *Langmuir* **1993**, 9, 1058– 1065, DOI: 10.1021/la00028a030
47. Sikiric, M.; Babic-Ivancic, V.; Milat, O.; Sarig, S.; Füredi-Milhofer, H. *Langmuir* **2000**, 16, 9261– 9266, DOI: 10.1021/la000704m

48. Galwey, A. K.; Brown, M. E. *Thermal Decomposition of Ionic Solids: Chemical Properties and Reactivities of Ionic Crystalline Phases*;Elsevier: Amsterdam, **1999**; Vol. 86.
49. Petrov, I.; Šoptrajanov, B.; Fuson, N.; Lawson, J. *Spectrochim. Acta, Part A* **1967**, 23, 2637– 2646, DOI: 10.1016/0584-8539(67)80155-7
50. Lecomte, J.; Boulle, A.; Langdupont, M. *C. R. Hebd. Seances Acad. Sci.* **1955**, 241, 1927– 1929
51. Arsic, J.; Kaminski, D.; Poodt, P.; Vlieg, E. *Phys. Rev. B: Condens. Matter Mater. Phys.* **2004**, 69, 245406, DOI: 10.1103/PhysRevB.69.245406
52. Penel, G.; Leroy, N.; Van Landuyt, P.; Flautre, B.; Hardouin, P.; Lemaitre, J.; Leroy, G. *Bone* **1999**, 25, 81S– 84S, DOI: 10.1016/S8756-3282(99)00139-8
53. Tortet, L.; Gavarri, J.; Nihoul, G.; Dianoux, A. *J. Solid State Chem.* **1997**, 132, 6– 16, DOI: 10.1006/jssc.1997.7383
54. Xu, J.; Butler, I. S.; Gilson, D. F. *Spectrochim. Acta, Part A* **1999**, 55, 2801– 2809, DOI: 10.1016/S1386-1425(99)00090-6
55. Schofield, P.; Knight, K.; van Der Houwen, J.; Valsami-Jones, E. *Phys. Chem. Miner.* **2004**, 31, 606– 624, DOI: 10.1007/s00269-004-0419-6
56. Chu, X.; Jiang, W.; Zhang, Z.; Yan, Y.; Pan, H.; Xu, X.; Tang, R. *J. Phys. Chem. B* **2011**, 115, 1151– 1157, DOI: 10.1021/jp106863q
57. Bromley, K. M.; Lakshminarayanan, R.; Thompson, M.; Lokappa, S. B.; Gallon, V. A.; Cho, K. R.; Qiu, S. R.; Moradian-Oldak, J. *Cryst. Growth Des.* **2012**, 12, 4897– 4905, DOI: 10.1021/cg300754a
58. Yang, X.; Sun, Z.; Ma, R.; Fan, D.; Moradian-Oldak, J. *J. Struct. Biol.* **2011**, 176, 220– 228, DOI: 10.1016/j.jsb.2011.07.016
59. Moradian-Oldak, J. *Matrix Biol.* **2001**, 20, 293– 305, DOI: 10.1016/S0945-053X(01)00154-8
60. Simmer, J. P.; Hu, J.C.-C. *Connect. Tissue Res.* **2002**, 43, 441– 449, DOI: 10.1080/713713530
61. Moradian-Oldak, J.; Paine, M. L.Mammalian Ename Formation *Biomineralization: From Nature to Application* **2010**, 4, 507– 546, DOI: 10.1002/9780470986325.ch15
62. Bromley, K. M.; Kiss, A. S.; Lokappa, S. B.; Lakshminarayanan, R.; Fan, D.; Ndao, M.; Evans, J. S.; Moradian-Oldak, J. *J. Biol. Chem.***2011**, 286, 34643– 34653, DOI: 10.1074/jbc.M111.250928
63. Curry, N.; Jones, D. *J. Chem. Soc. A* **1971**, 3725– 3729, DOI: 10.1039/j19710003725